

2005

Comparative study of oxide inclusion dissolution in CaO-SiO₂-Al₂O₃ slag

Brian J. Monaghan

University of Wollongong, monaghan@uow.edu.au

Liang Chen

University of Wollongong, lchen@uow.edu.au

J. Sorbe

Publication Details

Monaghan, BJ, Chen, L & Sorbe, J, Comparative study of oxide inclusion dissolution in CaO-SiO₂-Al₂O₃ slag, *Ironmaking and Steelmaking*, 32(3), 2005, p 258-264.

Comparative study of oxide inclusion dissolution in CaO–SiO₂–Al₂O₃ slag

B. J. Monaghan^{*1}, L. Chen² and J. Sorbe³

The dissolution of alumina, spinel and zirconia inclusions in a liquid CaO–SiO₂–Al₂O₃ slag has been investigated using laser scanning confocal microscopy. Over the experimental temperature range 1477–1577°C it is found that alumina inclusions have a slower dissolution rate than that of spinel, and that zirconia inclusions form gas bubbles at the inclusion surface during dissolution. The results have been analysed assuming mass transfer control in the slag phase, and the slower rate of dissolution of the alumina inclusions is explained by the observation that they have a greater mass of aluminium oxide, the rate controlling species, than that of spinel.

Keywords: Dissolution, Inclusions, Alumina, Spinel, Zirconia

Introduction

Oxide inclusions in steel are generally considered to be undesirable, as they are detrimental to its physical properties.¹ The inclusions are usually formed as reaction products from the steel deoxidation process, but may also result from slag or mould flux entrainment or refractory degradation. Typically the inclusions are removed by injection stirring techniques that promote contact between the inclusion and a slag.² The inclusion then dissolves in the slag. The rate at which an inclusion dissolves in the slag is a key parameter if predictive models are to be developed that quantitatively describe inclusion removal from steel.² Oxide dissolution kinetic studies^{3–13} have been traditionally conducted using techniques whereby a refractory material is dipped in slag and held for a period of time, removed, then analysed for slag corrosion and/or penetration. The dipped refractory sample may be static or rotated. Other data for MgAl₂O₄ spinel and alumina dissolution may be found in studies where the crucible was the refractory dissolution sample,¹⁴ or a known volume of powder was added to a slag.¹⁵ Where it was possible to evaluate the rate controlling mechanism of refractory dissolution,^{3–11,15} it was found that the dissolution was at least in part controlled by mass transfer in the slag phase. In the case of partially stabilised zirconia, it was found that the dissolution mechanism was mass transfer controlled at high basicities.¹³ With the exception of the powder addition experiments,¹⁵ all of these studies used large (macro)refractory samples and not microparticles more representative of inclusion dissolution for their experiments. This difference in scale could have a significant

bearing on the kinetics of dissolution of a solid oxide in a slag, and casts some doubt on whether observations and data measured for macrosystems can be applied to microsystems.¹⁶ Recently, a new technique, the high temperature laser scanning confocal microscope (LSCM),^{17–21} has become available, which offers possibilities of analysing the dissolution behaviour of inclusions in a slag directly. Studies using the LSCM^{17–21} have demonstrated that real time observations of the dissolution process in the bulk of a slag can be made, providing that the slag is transparent to the interrogation laser used in the instrument. Using this method it has been shown that dissolution investigations of macrorefractory systems are consistent with the general kinetic behaviour of microrefractory (inclusion) systems.^{17,19} Most macrodissolution studies have shown that alumina dissolution in CaO–SiO₂–Al₂O₃ is mass transfer controlled.^{3–11} This has been confirmed by LSCM observation of alumina inclusions dissolving in slag.^{17–19} There are much fewer data on MgAl₂O₄ spinel dissolution.^{3–5,14,19} Sandhage and Yurek^{3–5} found in their refractory MgO dissolution study that an intermediate MgAl₂O₄ spinel product was formed, and that the dissolution of this spinel product was at least in part mass transfer controlled in the slag phase. Valdez *et al.*¹⁹ studied spinel inclusion dissolution in CaO–SiO₂–Al₂O₃ using an LSCM and found their results to be consistent with mass transfer control. The present authors are unaware of any published LSCM investigations of zirconia dissolution. While there is consistency between the macro- and micro-oxide dissolution studies, there are still difficulties in scaling rate data from macro- to microscale. This difficulty arises from the poor descriptions of reaction area and flow conditions adjacent to the refractory/inclusion. Therefore, there is a need for kinetics data obtained from inclusion dissolution studies.

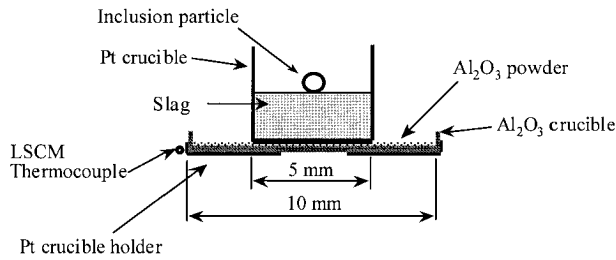
The present paper describes an investigation of the dissolution behaviour of alumina, spinel and zirconia inclusions in a CaO–SiO₂–Al₂O₃ slag using the LSCM.

¹School of Mechanical, Materials and Mechatronic Engineering and Steel Institute, University of Wollongong, Wollongong, NSW 2522, Australia

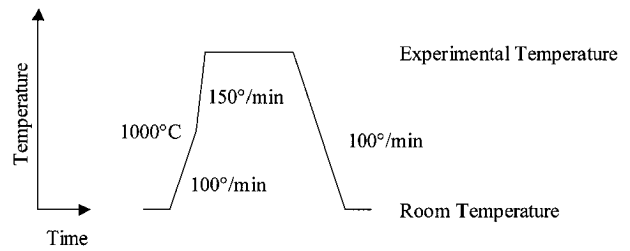
²Steel Institute, University of Wollongong, Wollongong, NSW 2522, Australia

³Institut National des Sciences Appliquées de Lyon, 20 rue Albert Einstein, 69621 Villeurbanne Cedex, France

*Corresponding author, email brian_monaghan@uow.edu.au



1 Schematic diagram of sample and crucible configuration in laser scanning confocal microscope (LSCM)



2 Schematic diagram of furnace heating profile used in LSCM experiments

Experimental

Experimental procedure

Experiments were carried out in a LSCM to observe and quantify the rate of dissolution of alumina, spinel and zirconia in a CaO–SiO₂–Al₂O₃ slag. Specific details of the LSCM technique have been widely published and are detailed elsewhere.^{17,18} A description follows of the procedure used and key experimental details. Inclusions were added to the cold fused slag as shown in Fig. 1, a schematic diagram of the sample holder and crucible setup used in the present study. The inclusion, sample holder and crucible were rapidly heated to the desired temperature in an infrared furnace and an air atmosphere. Once the slag was liquid, the inclusion was subducted by the slag and started to dissolve. The experiment ended when the inclusion was completely dissolved or some event took place that obscured direct observation of the dissolution process. The dissolving alumina and spinel inclusions were filmed using the LSCM and recorded to video. The zirconia inclusions were filmed using the LSCM and recorded to DVD. Temperature and time were logged throughout the experiment. The video and DVD were then subject to digital image analysis using Scan Image software²² to obtain inclusion dimensions. The heating profile used in all experiments is shown in Fig. 2. The LSCM was capable of magnifications of up to $\times 1350$, and could resolve inclusions down to sizes of $\sim 1 \mu\text{m}$ in diameter.

Experiments were carried out over the temperature range 1477–1577°C. A B type thermocouple was used for temperature measurement. To ensure accurate measurement, a temperature calibration was carried out whereby a type R thermocouple was welded to the side of the platinum crucible containing the slag material. This crucible, slag and type R thermocouple were placed in the LSCM and heated through the experimental temperature range. The difference between the LSCM and calibration thermocouple measurements was logged and used to correct the temperatures in subsequent experiments.

Digital analysis

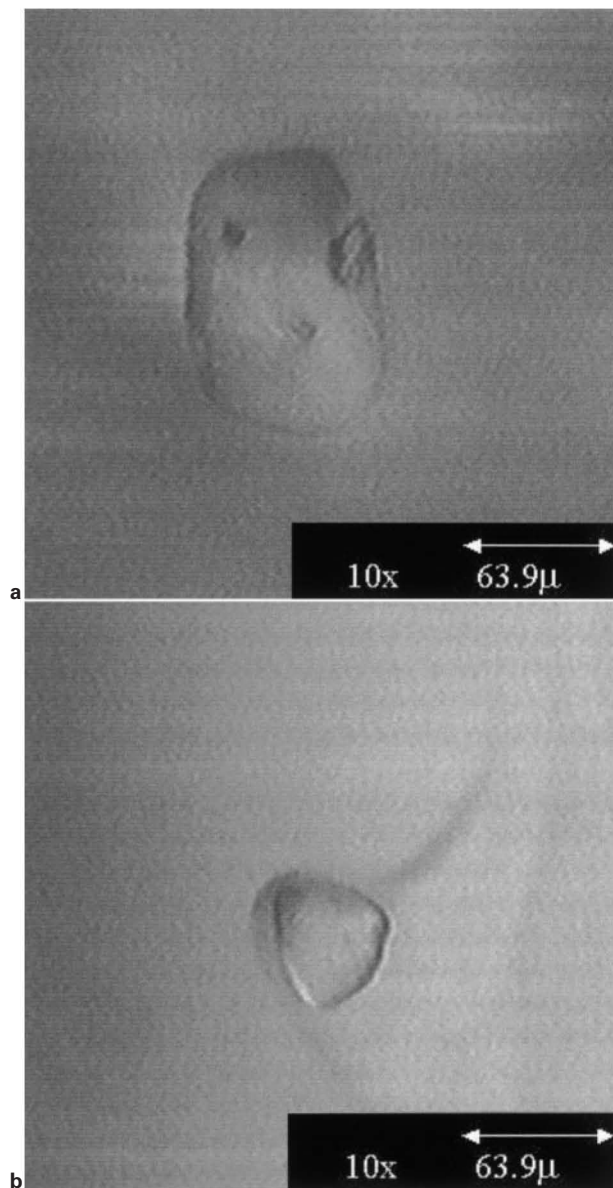
After each experiment the video and DVD recordings were analysed to obtain the change in inclusion area with time. The analysis procedure involved capturing and digitising image stills from the recordings then reading the digitised image into the Scan Image analysis software.²² Using this software, a border was manually drawn around the inclusion particle. This drawn object was then converted to an area. On the assumption that the particle was a sphere, a radius was then calculated from the area. This calculated radius formed the basis of the present results. The assumption that the particles were spheres introduced errors into the data analysis. As yet these errors have not been quantified and are the subject of another study. Mass transfer controlled dissolution is more sensitive to the geometry of the particle than is chemical reaction.¹⁶ It can therefore be expected that errors associated with the spherical particle assumption will have a greater impact on studies of a mass transfer controlled process. Examples of images obtained from the LSCM technique are shown in Fig. 3a and b for alumina and MgAl₂O₄ spinel, respectively.

Materials

The compositions of the alumina, spinel and zirconia inclusion particles and the slag used in the present study are given in Table 1. The reported slag composition is based on inductively coupled plasma (ICP) measurements. The alumina, spinel and zirconia particle compositions are based on batch analysis supplied by the manufacturers. The zirconia had a concentration of $> 99.9\%$ ZrO₂. The slag was prepared by premelting appropriate mixtures of CaO, SiO₂ and Al₂O₃, quenching the fused slag in water and then crushing the resultant glass. This process was repeated to obtain a homogeneous slag. The slag composition was chosen to ensure that it was transparent to the laser imaging system of the LSCM. Using a transparent slag enabled the inclusion dissolution process to be observed within

Table 1 Compositions of alumina, spinel and zirconia inclusion particles (wt-%) and slag used in present study

	CaO	SiO ₂	Al ₂ O ₃	MgO	ZrO ₂	Particle diameter, μm
Slag	16.3	64.5	19.3
Alumina particle	0.08	...	98.6	0.6	...	100
Spinel particle	72.7	28.3	...	80
Zirconia particle	> 99.9	100



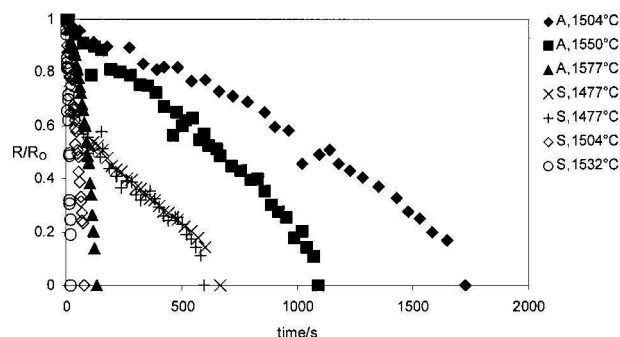
a alumina; b spinel
3 Typical images of inclusions obtained using confocal microscope

the bulk of the slag. The inclusion particles were sieved before use to obtain approximate particle sizes. The particle sizes are also listed in Table 1.

The inclusion compositions were chosen to represent deoxidation products (alumina and spinel) and refractory degradation products (spinel and zirconia).

Results

The results for alumina and MgAl₂O₄ spinel dissolution are shown in Fig. 4, where *R* represents the radius of the particle at time *t* and *R*₀ is the radius of the particle at time zero. Time zero is defined as the point at which the measured temperature reached the set experimental temperature. In Fig. 4 it can be seen that increasing the temperature increased the rate of dissolution of the inclusion particles, and also that the rate of spinel dissolution was greater than that of alumina. No dissolution data were obtained for zirconia. During the experiments, gas evolved during the inclusion



4 Alumina and spinel dissolution results: *R* radius of particle at time *t*, *R*₀ radius of particle at time zero, A alumina particles, S spinel particles

dissolution process, producing gas bubbles. These bubbles were attached to the zirconia inclusions and obscured the inclusion/refractory interface, preventing particle radius measurement. Figure 5 shows an image of the bubble formation during the zirconia dissolution process. Total dissolution time for a given temperature was similar to that of the alumina inclusions.

During the dissolution process the inclusion particles tended to rotate. It was not possible to measure the rate of rotation.

Discussion

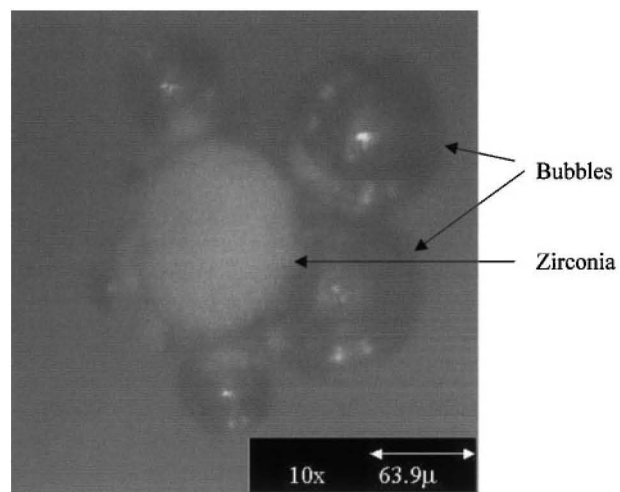
Alumina and spinel dissolution

Comparable studies by the present authors¹⁷ and other investigators^{18,19} of alumina and spinel inclusion dissolution found that the dissolution process was mass transport controlled in the slag phase. The results of the present investigation are discussed assuming this rate controlling mechanism.

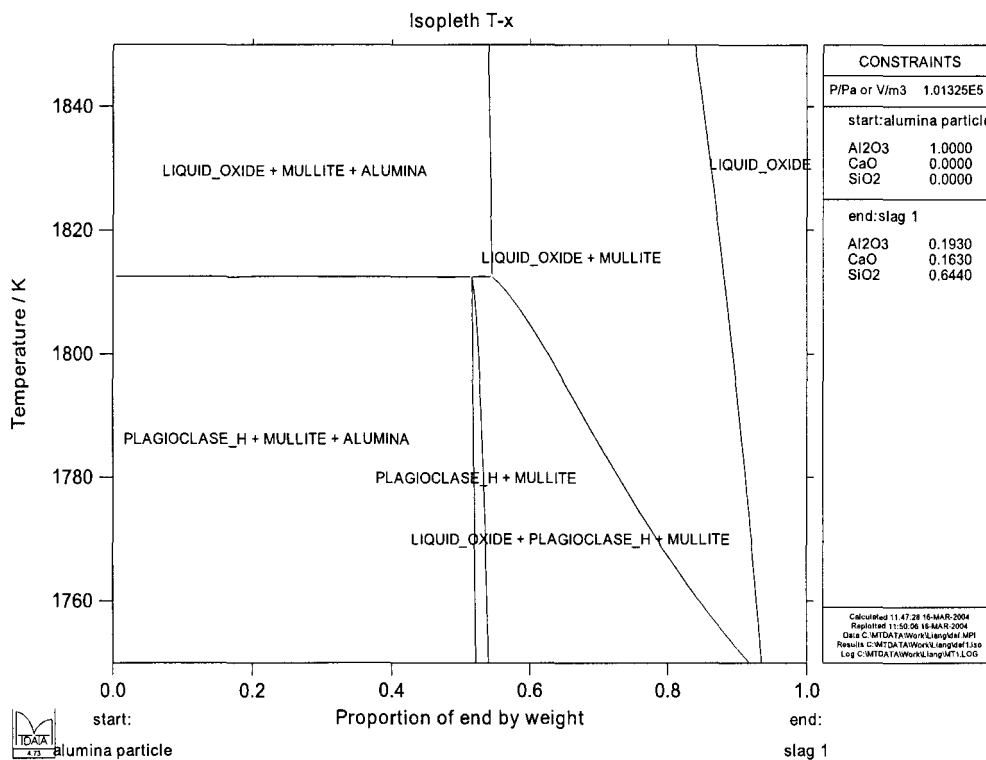
The effect of temperature can be explained by considering its influence on mass transport control in the slag phase. For a mass transport controlled process, Fick's law can be applied to diffusion across the stagnant boundary layer, giving

$$J = -D \frac{\Delta C}{\delta} \tag{1}$$

where *J* is the molar flux, *D* is the diffusion coefficient



5 Image showing bubble formation during zirconia dissolution



6 Isopleth sections calculated using MTDATA showing phase stability for given alumina inclusion–slag mixtures: start represents composition of alumina particle and end is slag composition 19.3%Al₂O₃, 16.3%CaO and 64.5%SiO₂

and ΔC is the concentration gradient across the boundary layer δ .

The diffusion coefficient D has an Arrhenius relationship with temperature according to

$$D = D_0 \exp(-A/RT) \quad (2)$$

where D_0 is a pre-exponential constant, A is the activation energy, R in this case is the gas constant and T is the temperature. From equation (2) it can be seen that increasing the temperature increases D and thereby increases J , the dissolution rate.

To explain why the spinel dissolves faster than the alumina is more difficult, as the dissolution rate is a function of particle radius, the thermodynamic driving force and the mobility of the diffusing species. Solutions to the shrinkage core model¹⁶ for mass transport control in the slag phase predict that the total time for a sphere to dissolve τ can be calculated from

$$\tau = \frac{R_0^2 \rho_{\text{particle}}}{2D(C_{\text{sat}} - C_{\text{bulk}})} \quad (3)$$

where ρ_{particle} is the density of the dissolving particle, C is the molar concentration and subscripts *sat* and *bulk* denote slag saturation and slag bulk composition, respectively. Providing that data are available to evaluate equation (3) and the rate limiting diffusion species is known, then it is possible to predict how long an inclusion particle will take to dissolve.

Isopleth sections for the inclusion–slag systems were calculated using MTDATA* to establish saturation limits, and are shown in Figs. 6 and 7 for alumina and

*MTDATA is a commercial thermodynamic software package developed at the National Physical Laboratory in the UK that is able to calculate complex multicomponent phase equilibria in gas–liquid–solid systems. It uses a Gibbs energy minimisation routine to establish the thermodynamic equilibrium of a defined system.

spinel inclusions, respectively.²³ The initial radius R_0 of the particles, alumina saturation composition and slag and particle densities are given in Table 2 for the experiments carried out at 1504°C. The parameter ΔC represents $(C_{\text{sat}} - C_{\text{bulk}})$ and is also given in Table 2. The particle densities were measured at 20°C using the pycnometer method, and corrected for expansion at higher temperatures using the Touloukian²⁴ and Morrel²⁵ reference data for alumina and spinel, respectively. The slag density was estimated using Slags Model software.²⁶

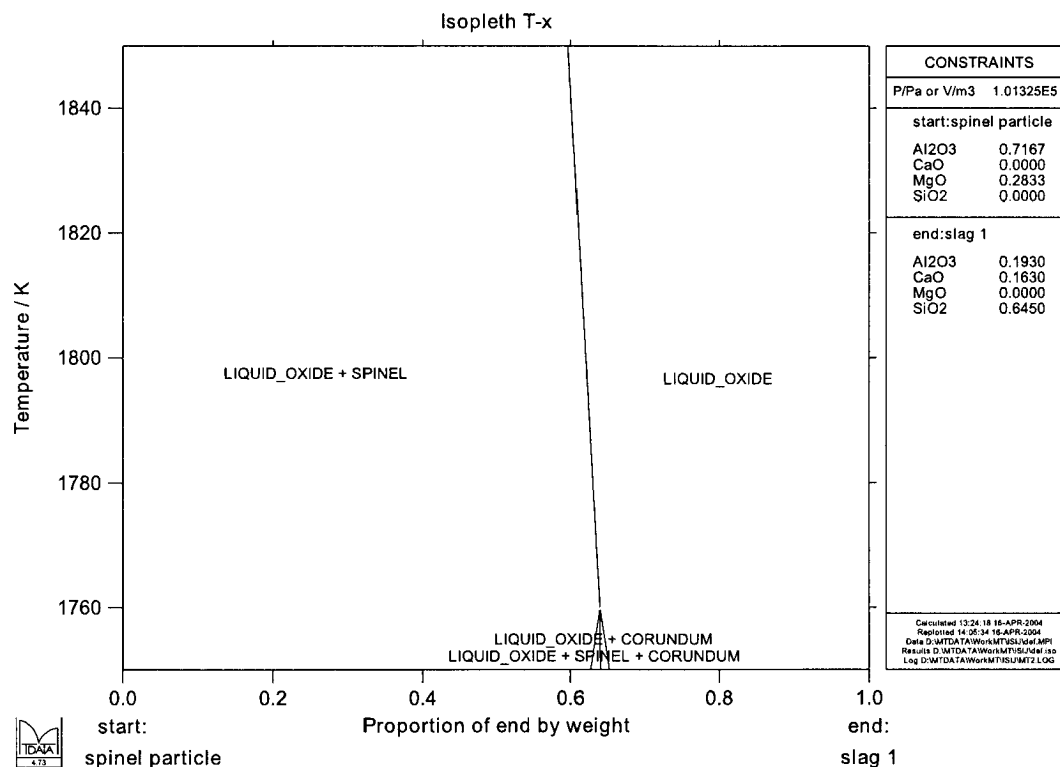
The data have been analysed assuming that an aluminium–oxygen anion is the rate limiting diffusion species in the slag phase for both alumina and spinel particles. That is, it is assumed that the aluminium–oxygen anion has a smaller diffusion coefficient than that of the magnesium cation.

The justification for this choice was based on the following.

1. The magnesium cation is smaller than the aluminium–oxygen ion complex.^{27,28} The consequences of this are best understood by considering the Eyring relationship²⁹ for diffusion

$$D = \frac{k_b T}{\eta \lambda} \quad (4)$$

where k_b is the Boltzmann constant, T is the temperature, η is the viscosity and λ is the jump distance of the diffusing species. The value of λ can be approximated to the radius of the diffusing ion. Inspection of equation (4) shows that, for all other items being equal, the smaller magnesium ion will have a larger diffusion coefficient. Therefore, the flux of magnesium is likely to be greater than that of aluminium and hence not rate controlling.



7 Isoleth sections calculated using MTDATA showing phase stability for given spinel inclusion-slag mixtures: start represents composition of spinel particle and end is slag composition 19.3%Al₂O₃, 16.3%CaO and 64.5%SiO₂

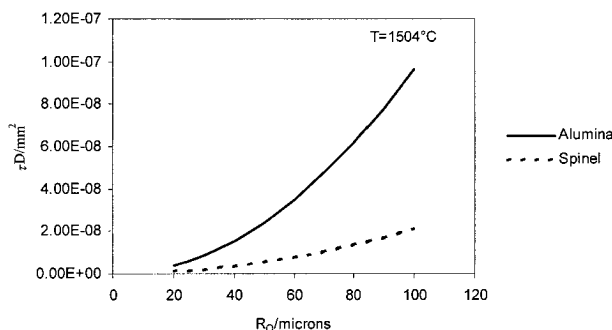
2. Where comparable data are available, magnesium has a greater diffusion coefficient than that of aluminium and therefore will have a faster diffusive flux and not be rate controlling: compare $4.6 \times 10^{-9} \text{ m}^2 \text{ s}^{-1}$ for magnesium in a 20%Al₂O₃-40%SiO₂-40%CaO (wt-%) slag at 1504°C with $2.2 \times 10^{-11} \text{ m}^2 \text{ s}^{-1}$ for aluminium in a 20%Al₂O₃-41%SiO₂-39%CaO slag at 1504°C.²⁸

Without diffusion data it is impossible to evaluate equation (3) directly, but if experiments were carried out at the same temperature and the same diffusion species was rate controlling, then the diffusion coefficient for the rate controlling species would be constant. Under such conditions, evaluation of τD , i.e.

$$\tau D = \frac{R_0^2 \rho_{\text{particle}}}{2(C_{\text{sat}} - C_{\text{bulk}})} \quad (5)$$

would enable prediction of the relative rate of dissolution of the alumina or spinel inclusions in the slag. The values of τD at 1504°C for alumina and spinel inclusions are $3.2 \times 10^{-8} \text{ m}^2$ and $2.6 \times 10^{-9} \text{ m}^2$, respectively, indicating that the alumina would take longer to dissolve. This is consistent with the experimental data.

To assess whether this is primarily an inclusion size effect, τD values have been calculated as a function of



8 Relative rate of dissolution τD plotted as function of initial particle size R_0 : T temperature

initial particle size, the results being shown in Fig. 8. The same assumptions as used above when evaluating equation (5) apply. From Fig. 8 it can be seen that even if the particles were the same size the alumina would take longer to dissolve. Given that there is less of a thermodynamic driving force, represented by $(C_{\text{sat}} - C_{\text{bulk}})$ in equation (5), and noted as ΔC in Table 2, for the spinel to dissolve, perhaps it would be expected that the spinel inclusion would have a slower rate of dissolution than that

Table 2 Initial radius R_0 of particles, alumina saturation composition $C_{\text{Al}_2\text{O}_3}$, slag and particle densities and ΔC ($= C_{\text{sat}} - C_{\text{bulk}}$, where C_{sat} is saturation and C_{bulk} is bulk molar concentration of slag) for experiments carried out at 1504°C

	$R_0, \mu\text{m}$	Density, kg m^{-3}	$C_{\text{Al}_2\text{O}_3}, \text{mol m}^{-3}$	$\Delta C, \text{mol m}^{-3}$
Slag	...	2500	4730	...
Alumina inclusion, saturated slag	...	2541	6545	1815
Spinel inclusion, saturated slag	...	2659	10061	5330
Alumina particle	57.3	3574
Spinel particle	35.3	3194

of alumina. This is not the case: the principal reason that the spinel inclusion dissolves faster is that there is less mass of aluminium oxide, the rate controlling diffusing species, to dissolve.

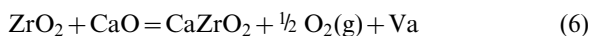
Zirconia dissolution

It was not possible to measure the dissolution rate of the zirconia inclusion as the particle/slag interface was obscured by gas bubble formation. Possible sources of gas causing bubble formation on the particle could be:

- (i) bubbles in the slag migrating and attaching to the particle
- (ii) gas supersaturation of the slag, resulting in nucleation of gas bubbles on the zirconia particle
- (iii) the particle having a hollow centre, and the possibility of gas entrained within the particle leaching out during the dissolution experiment
- (iv) reaction between the zirconia sample and the slag forming a gas.

The first three possibilities have been ruled out because there were few or no gas bubbles in the slag away from the particle before bubble appearance, no bubble formation was found when using other inclusion particles under the same conditions and crushed zirconia particles also exhibited bubble formation. Also, using zirconia particles without a hollow centre, i.e. of a higher density, resulted in similar bubbling behaviour to that with hollow centre zirconia particles. Preliminary work on yttria partially stabilised zirconia also showed bubble formation, although the bubble growth rate appeared to be slower. More work is required to confirm this observation.

What could not be ruled out was the possibility that the zirconia was reacting with the slag to produce the gas bubbles. For example, zirconia can absorb calcium from slag to form a solid solution



where Va represents a vacancy within the CaZrO₂ structure.³⁰ On the assumption that there is no resistance to bubble formation; the pressure in the bubble is equal to the furnace atmosphere pressure (1 atm), and ignoring the energy required to form a bubble, the ZrO₂ would only have to adsorb ~1 ppm of calcium to result in an oxygen bubble of 10 μm radius at 1450°C. It is likely that a reaction similar in nature to that given in equation (6) is responsible for the bubble generation.

The effect of bubble formation on the dissolution kinetics cannot be ignored, as it will act as a barrier to zirconia dissolution in slags. The primary conclusion from this LSCM study of zirconia dissolution in the slag composition used is that the LSCM is not a suitable apparatus to measure the reaction kinetics, although it can be used to observe phenomena important in delineation of the kinetics.

Effect of particle rotation on dissolution

In the present and another study¹⁹ of inclusion dissolution into slag, the inclusion has been observed to rotate during the dissolution process. The effect of this rotation is likely to be significant for any mass transfer controlled dissolution process and any model that attempts to predict the dissolution kinetics. Increasing the relative

velocity of the fluid surrounding the inclusion would reduce the stagnant boundary layer δ as defined in equation (1). Reducing δ would increase the molar flux J , i.e. increase the rate of dissolution. The rotation is an important observation, as this phenomenon will also occur in industrial processes. It is likely that the inclusion rotation is due to Marangoni (interfacial tension driven) flow.³¹ Marangoni flow can be described by

$$F = \frac{d\gamma}{dx} = \frac{\partial\gamma}{\partial C} \frac{dC}{dx} \quad (7)$$

where F is the shear force on the fluid generated by a composition gradient, x is the distance, γ is the interfacial tension and C in this case is composition.

If an accurate description of the inclusion dissolution process in slag is required, then the effects of Marangoni flow, in addition to other slag flow, on the rate of dissolution will need to be considered. Traditional measurements of the rate of refractory dissolution in slags using dip techniques will not readily replicate the effect of inclusion rotation due to Marangoni flow. This may lead to poor predictions of inclusion dissolution rates if data based on dip techniques are used.

Conclusions

The rate of dissolution of alumina inclusions in the CaO–SiO₂–Al₂O₃ slag composition used in the present study is slower than that of spinel. This is principally because there is a greater mass of aluminium oxide in the alumina inclusion than there is in spinel to dissolve.

Owing to bubble formation on the zirconia particle it was difficult to evaluate its dissolution kinetics using the LSCM. While this limited the quantitative information obtained from the experiments, it highlighted important phenomena that must be taken into account should a rigorous description of zirconia dissolution be required.

Acknowledgements

The authors wish to thank their University of Wollongong colleagues, Dr S. Nightingale, Professor R. Dippenaar, Dr D. Phelan and Mr M. Reid, and Bluescope Steel, for support both for and during this study.

References

1. J. H. Lowe and A. Mitchell: 'Clean steel', 223–232; 1995, London, Institute of Materials.
2. B. Dea and R. Boom: 'Fundamentals of steelmaking metallurgy', 84–96; 1993, New York, Prentice Hall International.
3. K. Sandhage and G. Yurek: *J. Am. Ceram. Soc.*, 1990, **73**, 3633–3642.
4. K. Sandhage and G. Yurek: *J. Am. Ceram. Soc.*, 1990, **73**, 3643–3649.
5. K. Sandhage and G. Yurek: *J. Am. Ceram. Soc.*, 1988, **71**, 478–489.
6. S. Taira, K. Nakashima and K. Mori: *ISIJ Int.*, 1993, **33**, 116–123.
7. S. Taira, A. Machida, K. Nakashima and K. Mori: *J. Iron Steel Inst. Jpn*, 1996, **82**, 1–5.
8. K. Ueda: *J. Jpn Inst. Met.*, 1999, **63**, 989–993.
9. X. Yu, R. J. Pomfret and K. S. Coley: *Metall. Mater. Trans. B*, 1997, **28B**, 275–279.
10. J. Y. Choi, H. G. Lee and J. S. Kim: *ISIJ Int.*, 2002, **42**, 852–860.
11. A. R. Cooper and W. D. Kingery: *J. Am. Ceram. Soc.*, 1964, **47**, 37–43.
12. A. F. Dick, R. J. Pomfret and K. S. Coley: *ISIJ Int.*, 1997, **37**, 102–108.

13. Y. D. Chung and M. E. Schlesinger: *J. Am. Ceram. Soc.*, 1994, **77**, 611–616.
14. K. Goto, B. B. Argent and W. E. Lee: *J. Am. Ceram. Soc.*, 1997, **80**, 461–471.
15. W. D. Cho and P. Fan: Proc. EPD Cong. and ‘Fundamentals of advanced materials for energy conversion’, Seattle, WA, USA, February 2002, TMS, 631–638.
16. O. Levenspiel: ‘The chemical reactor omnibook’, 51.1–51.6; 1989, Oregon, USA, OSU Book Stores.
17. B. J. Monaghan, S. A. Nightingale, L. Chen and G. A. Brooks: Proc. VII Int. Conf. on ‘Molten slags and fluxes and salts’, Johannesburg, South Africa, January 2004, SAIMM, 585–594.
18. S. Sridhar and A. W. Cramb: *Metall. Mater. Trans. B*, 2000, **31B**, 406–410.
19. M. Valdez, K. Prapakorn, A. W. Cramb and S. Sridhar: *Steel Res.*, 2001, **72**, 291–297.
20. S. H. Lee, C. Tse, K. W. Yi, P. Misra, V. Chevrier, C. Orrling, S. Sridhar and A. W. Cramb: *J. Non-Cryst. Solids*, 2001, **282**, 41–48.
21. D. J. Phelan and R. J. Dippenaar: Proc. ‘The Brimacombe Memorial Symposium’, Vancouver, Canada, October 2000, TMS, 579–593.
22. L. R. Jarvis: *J. Microsc.*, 1988, **150**, 83–97.
23. R. H. Davies, A. T. Dinsdale, J. A. Gisby, S. M. Hodson and R. G. J. Ball: Proc. Conf. ‘Applications thermodynamics in the synthesis and processing of materials’, Rosemont, IL, USA, 1994, ASM/TMS, 371–384.
24. Y. S. Touloukian, R. K. Kirby, R. E. Taylor and T. Y. R. Lee: ‘Thermophysical properties of matter’, Vol. 13, 176; 1977, New York, IFI/Plenum.
25. R. Morrell: ‘Handbook of properties of technical and engineering ceramics’, Part 1, 77–82; 1989, London, Her Majesty’s Stationery Office.
26. K. C. Mills: Slags Model, Version 1.07, National Physical Laboratory, London, UK, 1986.
27. ‘CRC handbook of chemistry and physics’, 1997, London, CRC Press.
28. K. C. Mills (ed.): ‘Slag atlas’, 2nd edn, 349–353; 1995, Düsseldorf, Germany, Verlag Stahleisen.
29. D. R. Poirier and G. H. Geiger: ‘Transport phenomena in materials processing’, 444–453; 1994, Warrendale, PA, TMS.
30. E. D. Wachsman, F. E. G. Henn, N. Jiang, P. B. Leezenberg, R. M. Buchanan, C. W. Frank, D. A. Stevenson and J. F. Wenckus: ‘Science and technology of zirconia’, Vol. V, 584–592; 1993, Basel, Switzerland, Technomic Publishing.
31. K. Mukia: *Philos. Trans. R. Soc. (London) A*, 1998, **A356**, 1015–1021.